Mesoporous Piezoelectric Polymer Composite Films with Tunable Mechanical Modulus for Harvesting Energy from Liquid Pressure Fluctuation

*Zhiyi Zhang, Chunhua Yao, Yanhao Yu, Zhanglian Hong, Mingjia Zhi, and Xudong Wang**

Harvesting mechanical energy from biological systems possesses great potential for in vivo powering implantable electronic devices. In this paper, a development of flexible piezoelectric nanogenerator (NG) is reported based on mesoporous poly(vinylidene fluoride) (PVDF) films. Monolithic mesoporous PVDF is fabricated by a template-free sol–gel-based approach at room temperature. By filling the pores of PVDF network with poly(dimethylsiloxane) (PDMS) elastomer, the composite's modulus is effectively tuned over a wide range down to the same level of biological systems. A close match of the modulus between NG and the surrounding biological component is critical to achieve practical integration. Upon deformation, the composite NG exhibits appreciable piezoelectric output that is comparable to or higher than other PVDF-based NGs. An artificial artery system is fabricated using PDMS with the composite NG integrated inside. Effective energy harvesting from liquid pressure fluctuation (simulating blood pressure fluctuation) is successfully demonstrated. The simple and effective approach for fabricating mesoporous PVDF with tunable mechanical properties provides a promising route toward the development of self-powered implantable devices.

1. Introduction

The recent invention and rapid evolution of piezoelectric nanogenerator (NG) represents a very promising strategy for environmental mechanical energy harvesting.[1–3] A large variation of creative NG designs have enabled the harvesting of various mechanical energy sources, such as acoustic waves, random vibrations, and even biological activities.[4–13] Among all proposed application directions, harvesting biomechanical energy possesses a very unique potential due to the great desire of self-powering capability of implantable devices and the extremely limited access to other possible energy sources in human body. In order to achieve effective biomechanical energy harvesting, the NG needs to be highly flexible and stretchable, so that the NG could be conformally attached to the irregular and soft surfaces of biological systems. Such a high flexibility could be realized by reducing the size down to nanometer scale and/or selecting flexible polymeric materials. For example, ZnO nanowires and $BaTiO_3$ were integrated with polymer matrix, such as poly(dimethylsiloxane) (PDMS) to achieve good flexibility to be used on the surface of heart.[14–20] Ultrathin ferroelectric (lead zirconate titanate) PZT films were also integrated on flexible substrate to achieve seamless contact with tissue surface to harvesting mechanical energy from heart beating and breathing.[21,22] As a high-performance piezoelectric polymer, poly(vinylidene fluoride) (PVDF) was frequently used directly as a flexible mechanical energy harvesting component without the support of flexible substrate.[23–25]

Nevertheless, it is known that for any implantable device, if coordinated movement is needed, the mechanical properties have to match those of the supporting biological component. That is, for an implantable NG, the modulus needs to match that of muscle/tissue/bone systems in order to prevent any stress shielding effect. Although submicrometer-scale ceramic materials were generally used to achieve good flexibility in NG designs, their Young's moduli, which are typically orders of magnitude higher than that of muscle or organs, remained unchanged. The piezoelectric polymer materials, such as PVDF, have much lower modulus compared to ceramics, whereas it is still one order of magnitude higher than the biological components. Due to the requirement of crystalline phase in order to show aligned polarization, the piezoelectric polymers typically have much limited elasticity compared to regular elastomers. The large mismatch between flexible NG devices and living biological systems would impose a tremendous obstacle for practical application of flexible NGs as an implantable powering device. A few recent developments revealed that introducing

Z. Zhang, C. Yao, Y. Yu, Prof. X. Wang
Department of Materials Science and Engineering
University of Wisconsin-Madison
Madison, WI 53706, USA
E-mail: xudong.wang@wisc.edu
Z. Zhang, Prof. Z. Hong, Prof. M. Zhi
State Key Laboratory of Silicon Materials
School of Materials Science and Engineering
Zhejiang University
Hangzhou 310027, China

DOI: 10.1002/adfm.201602624

porosity to piezoelectric PVDF films could effectively tune the films' mechanical property while achieve appreciable electric output.[26–29] Although the overall elasticity was sacrificed to a certain level due to pore involvement, the mesoporous polymeric structure is still a very promising solution to mechanical property optimization for implantable systems. In this paper, we report a development of large area mesoporous PVDF films via a template-free sol–gel-based approach. Elastomer PDMS was infiltrated into the PVDF network and achieved excellent elasticity and Young's modulus tuning to the level of biological systems, such as blood vessels. Appreciable electric output was obtained from the flexible and transparent polymer composite NGs. An artificial arterial system was fabricated with a PVDF-PDMS NG integrated and the capability of harvesting energy from liquid pressure fluctuation (simulating blood pressure fluctuation) was successfully demonstrated.

2. Results and Discussion

The mesoporous PVDF network was fabricated by a sol–gel method and the fabrication processes are schematically illustrated in **Figure 1**a (see the Experimental Section for details). This process started with PVDF/dimethyl sulfoxide (DMSO) gels obtained by keeping the PVDF/DMSO solution at 12 °C for 2 h. Drying the PVDF/DMSO gels in vacuum (0.8 Pa) at room temperature (18–25 °C) completely removed DMSO and yielded a mesoporous PVDF network. As shown in Figure 1b, the as-received PVDF foam surface (4% PVDF) exhibited an interconnected network feature with observable pore size from nearly 1 μm to 100 nm. This fabrication strategy is very simple and advantageous in effectively producing high-porosity PVDF films without using any templates. Compared to other regularly used solvents, such as *N,N*-dimethylformamide, *N,N*-dimethylacetamide (DMAc), and acetone (which typically led to PVDF shrinkage during the removal of the liquid media), DMSO has higher melting point, and thus the PVDF/DMSO gel could remain solid at relatively high temperature allowing DMSO being removed via sublimation in vacuum. Absence of the liquid phase eliminated the capillary force during drying, and thereby significantly suppressed the gel network shrinkage and well preserved the porous structure. Through this approach, PVDF networks were fabricated with a wide range of PVDF volume ratio from 3% to 18%. All of the samples exhibited highly porous structure and corresponding scanning electron microscopy (SEM) images are given in Figure S1 (Supporting Information). The nitrogen adsorption–desorption isotherm confirmed that the pore volume monotonically decreased as the PVDF fraction increased (Figure S2, Supporting Information). This measurement also showed that the pore volume distributions were very similar amount these samples with different PVDF volume fractions. The much larger sized pores in SEM were probably just a result of surface pore agglomeration. The stable pore size distribution was possibly a manifestation of the equilibrium droplet size of solid DMSO solvent controlled by the interfacial surface tension during solidification.

Fourier transform infrared (FTIR) spectrum was conducted to confirm the existence of the ferroelectric β-phase in the porous PVDF slabs. The characteristics absorption peaks of the β-phase at 840 and 1280 cm^{-1} appeared from all the samples (Figure S3a, Supporting Information), suggesting the presence of appreciable amount of the β-phase regardless of the PVDF fraction.[30,31] X-ray energy dispersive spectroscopy spectrum further revealed that the porous PVDF contained only C and F (Figure S3b, Supporting Information), confirming the complete removal of the DMSO solvent. The as-prepared

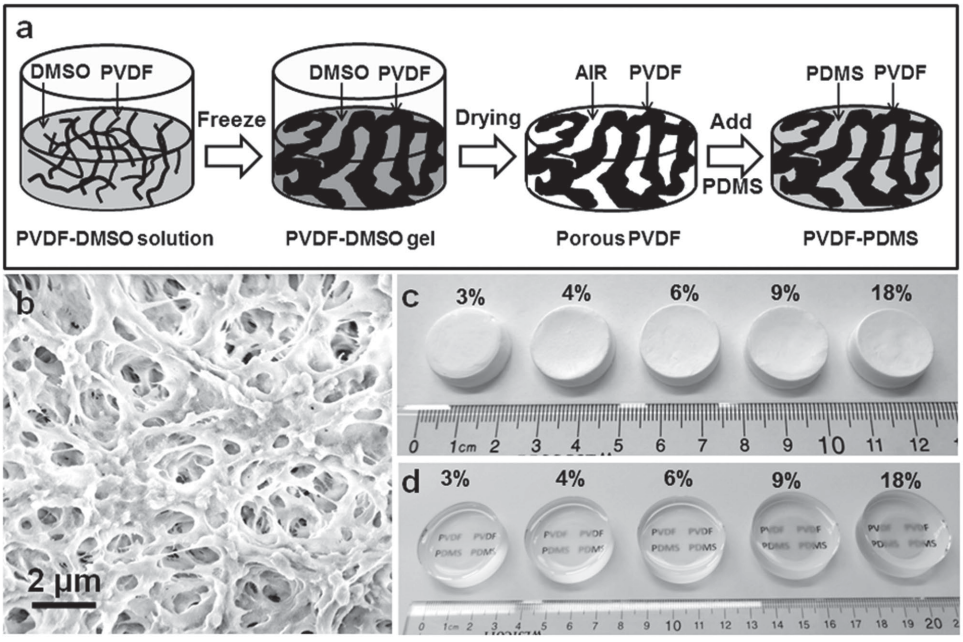

Figure 1. a) Schematic procedure of preparing mesoporous PVDF-PDMS composite film. b) SEM image showing the high porosity from the PVDF film with 4% volume fraction. c) Digital photos of porous PVDF with different PVDF volume fractions, and d) corresponding PVDF-PDMS composites showing good transparency particularly at low PVDF ratios.

Adv. Funct. Mater. **2016**,
DOI: 10.1002/adfm.201602624

mesoporous PVDF slabs were white, foam-like and can be made in large scale. 20 mm wide and 5 mm thick samples with different PVDF volume fraction (3%–18%) are shown in Figure 1c. The density of the porous PVDF slabs increased from 0.047 to 0.306 g cm^{-3} with the increase of PVDF fraction. The white porous PVDF slabs turned into transparent after being infiltrated with PDMS and the transparency slightly decreased when the PVDF volume fraction was above 9% (Figure 1d). Corresponding UV–vis transmission spectra were presented in Figure S4 (Supporting Information). More PVDF introduced more scattering and this effect was significant at shorter wavelength range. It was also interesting to observe that all infiltrated samples exhibited slightly higher transmittance when the scattering effect became insignificant (i.e., at longer wavelength). This enhancement could be attributed to the antireflection effect due to the mixed heterostructure.[32]

While the mechanical stiffness is directly related to the volume fraction of PVDF, infiltration of PDMS could largely improve their elasticity and tune their mechanical strength. Thus, mechanical property of the composite polymer slabs was studied first. The PVDF-PDMS composite slabs with different PVDF volume fraction were prepared in identical dumbbell shape (Figure S4, Supporting Information) and circular disk (Figure S5, Supporting Information) for tensile and compressive test, respectively. The tensile and compressive tests were conducted at a displacement rate of 20 mm min^{-1} and the corresponding strain–stress curves are shown in **Figure 2**a,b, respectively. From the tensile test, all the samples exhibited elastomer-type behavior, while increasing the PVDF fraction significantly raised the material's stiffness. The fracture strain rapidly decreased from ≈50% at 3% PVDF to <10% when the PVDF fraction was greater than 9% (Figure 2a). The tensile moduli of the PVDF-PDMS samples were calculated from the linear elastic region of stress/strain curves following the Hooke's law. As shown in Figure 2c, the tensile modulus increased from 0.8 to 30.16 MPa (tensile modulus of pure PDMS modulus is 0.12) with the increase of PVDF volume fraction. This modulus range covered the modulus of certain human organs, such as blood vessel, which was known to be in the range of 0.1–1 MPa.[33] The compressive moduli was calculated at the strain range <10%. As shown in Figure 2d, the compressive moduli increased monotonically from 21.95 to 36.58 MPa with the increase of PVDF volume fraction. For pure PVDF films, the tensile and compressive moduli were identified to be 318 and 409.5 MPa, respectively (Figures S6 and S7, Supporting Information). This comparison demonstrated that the mesoporous PVDF-PDMS composite structure could significantly improve the elasticity of the piezoelectric slab and bring the modulus down to the same level of biological systems.

The tunable mechanical property endowed unique advantages to the ferroelectric polymer composite slabs for mechanical energy harvesting. To test the porosity-related piezoelectric output, a simple NG was fabricated by attaching copper foil electrodes onto both sides of the PVDF-PDMS slab. The NG slab was placed on a flat hard surface with a constant mechanical force applied to the top surface at certain frequencies (Figure S8, Supporting Information). **Figure 3**a,b shows the open-circuit voltage (V_{oc}) and short-circuit current (I_{sc}) collected from the 4%PVDF-PDMS NG slab, respectively, under a force of 6 N and at a frequency of 20 Hz. The contact area between the applied force and NG was 0.2 cm^2, which gave a pressure of 0.3 MPa. Under this condition, the average peak values of the V_{oc} and I_{sc} were found to be about 2.87 V and 3.42 μA, respectively. Even with significant less PVDF fraction due to the highly porous structure, the obtained output voltage and current were still comparable or even higher than that of other PVDF-based NGs reported previously.[34–36] The higher piezoelectric response is probably owing to the large amount of pure and highly crystalline β-phase PVDF at the pore interface.[27]

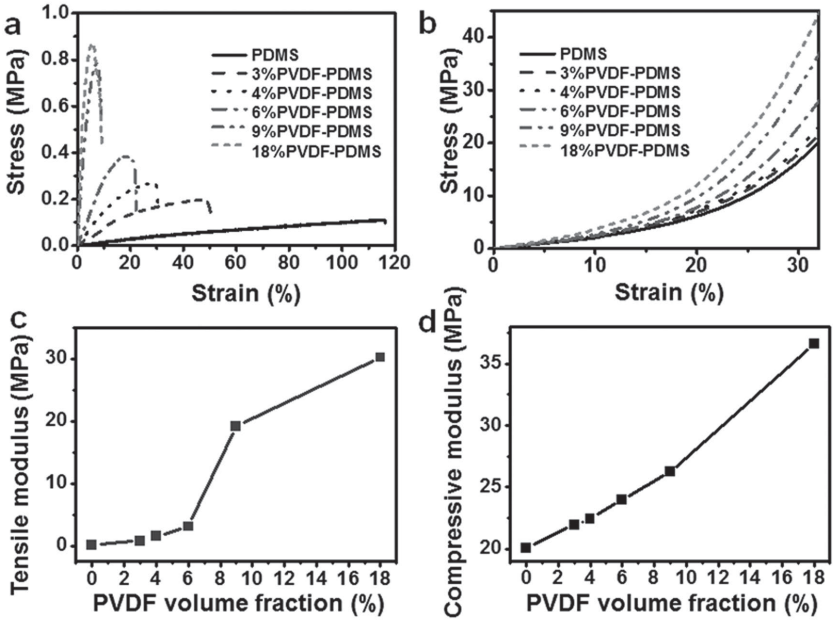

Figure 2. a) Tensile stress/strain curves and b) compressive stress/strain curves of PDMS and mesoporous PVDF-PDMS composites with different PVDF volume fractions. Calculated Young's moduli of the PVDF-PDMS composites under c) tensile and d) compressive strains.

To understand how the variation of mechanical property influences the piezoelectric output, PVDF-PDMS NG slabs fabricated with a series PVDF volume fraction (3%–18%) were characterized under identical conditions. Under an impact frequency of 20 Hz, the average peak values of V_{oc} were plotted as a function of PVDF volume ratio (square dots in Figure 3c). Corresponding voltage output profiles were included in Figure S9 (Supporting Information). The 4%PVDF-PDMS NG slab exhibited the highest piezoelectric output with a peak V_{oc} of 2.87 V. As the PVDF volume fraction increased from 4% to 18%, V_{oc} quickly dropped from 2.87 to 0.22 V. To understand this phenomenon, the strain subjected by the NG slab was extracted from the stress–strain curves under 6 N force. As shown by the triangle dots in Figure 3c, the strain decreased monotonically from 1.37% to 0.82% when the volume fraction of PVDF

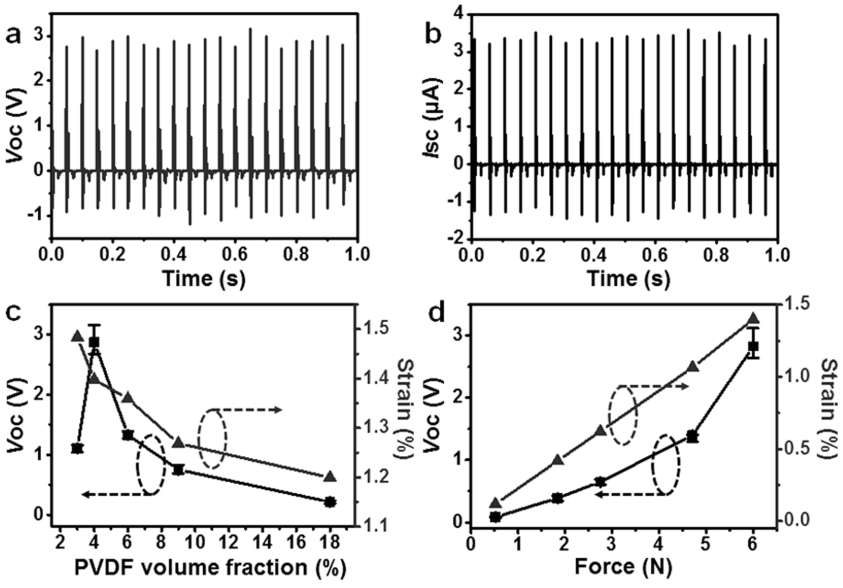

Figure 3. a) Piezoelectric output voltage and b) current profiles measured from a 4% PVDF-PDMS NG slab under a periodic 6 N compressive force. c) Peak V_{oc} (squares) and corresponding strain subjected by the NG slab (triangles) as a function of the PVDF volume fraction obtained under the same 6 N compressive force. d) Peak V_{oc} (squares) and corresponding strain subjected by the NG slab (triangles) as a function of the applied force obtained from the 4% PVDF-PDMS NG.

increased from 3% to 18%. Because the electric displacement is directly related to the strain, the piezoelectric output would exhibit similar monotonic decrease if other factors remained constant. Nevertheless, the piezoelectric output is also directly proportional to the PVDF volume fraction, which would result a monotonic increase of the V_{oc} as PVDF volume fraction increases. Both effects implemented simultaneously and yielded the optimal situation at the PVDF fraction of 4%.

For the best-performance 4% PVDF-PDMS NG, force/strain-related output was further tested. The force applied to the NG slab was increased from 0.52 to 6 N. Given the stress–strain relation shown in Figure 2b, the strain subjected by the NG slab would increase linearly from 0.12% to 1.34% (triangle dots in Figure 3d). Nevertheless, although the peak V_{oc} exhibited a monotonic increase following the force, a more rapid increase was observed under large compressive forces (square dots in Figure 3d), possibly a result of nonlinear increase of the straining rate from the actuator. Corresponding long-term operation V_{oc} profiles at a frequency of 20 Hz and different force applied to top surface of the PVDF-PDMS device are shown in Figure S10 (Supporting Information).

Basic mechanical and piezoelectric characterizations revealed the capability of tuning the NG modulus to the level of biological systems and meanwhile generating appreciable piezoelectric output. Therefore, the mesoporous piezoelectric polymer-based composite slabs may exhibit unprecedented application potential as organ attachment or replacement for harvesting energy from liquid pressure fluctuation (simulating blood pressure change). Blood pressure fluctuation is a regular and constant mechanical energy source in human body. To demonstrate the capability of harvesting this type of energy, a sealed cylindrical tube was fabricated mimicking the blood vessel using PDMS with a PVDF-PDMS NG imbedded inside the wall (**Figure 4**a). Thin sheets of copper electrode were applied on both sides of the NG slab. The artificial artery system was assembled by connecting the flexible energy-harvesting tube with a computer-controlled syringe pump, which pumped water in and out from the tube to mimic the process of heart beating-induced blood pressure change (Figure 4b and video S1, Supporting Information). As shown in the right panel of Figure 4a, when water was pumped in, the tube subjected to a high internal pressure and the NG slab was stretched and bent outward. While water was pumped out, the negative internal pressure retracted the flexible walls and compressed the PVDF NG making it bending inward. This process simulated the blood pressure variation and produced alternative electric polarization on both electrodes. The output voltage was thus recorded under a continuous pressure oscillating at a frequency of 1 Hz (simulating normal heart beating, Video S2, Supporting Information). As shown in Figure 4c, the average peak-to-peak voltage was ≈0.35 V when the internal water pressure difference (ΔP) was 100 kPa. The inset of Figure 4c shows an enlarged individual voltage pulse, where a positive voltage was obtained first, consistent with the polarization direction and straining situation of the PVDF film. The positive voltage peaks were typically ≈150 mV larger than the negative peaks, possibly due to the slightly slower retraction rate of the polymer wall.

To further investigate the energy harvesting capability, a series of ΔP was applied to the artificial arterial system at a constant rate of 60 min^{-1}. It was found that the piezoelectric output increased with the increase of ΔP (Figure S11, Supporting Information) and the average peak-to-peak values of the V_{oc} raised from 0.25 to 1.27 V when ΔP increased from 60 to 158 KPa (Figure 4d). The piezoelectric output was also measured within the range of normal heart beating rates at a constant ΔP of 113 KPa and different frequencies (Figure S12, Supporting Information). The average peak-to-peak values of the V_{oc} increased monotonically from 0.07 to 0.83 V when the frequency increased from 15 to 120 min^{-1} revealing the positive influence of the straining rate to the piezoelectric output.

3. Conclusion

In summary, we demonstrated an effective strategy of preparing mesoporous piezoelectric β-phase PVDF film at room temperature using high-melting-point solvent DMSO. By controlling the porosity of PVDF network and filling the pores with elastic PDMS, the Young's modulus of the PVDF-PDMS composite film was significantly reduced down to the same level of human blood vessel while retaining appreciable piezoelectric output. Due to the combined effects of modulus and PVDF volume ratio, the best performance was found from the composition of

Adv. Funct. Mater. **2016**,
DOI: 10.1002/adfm.201602624

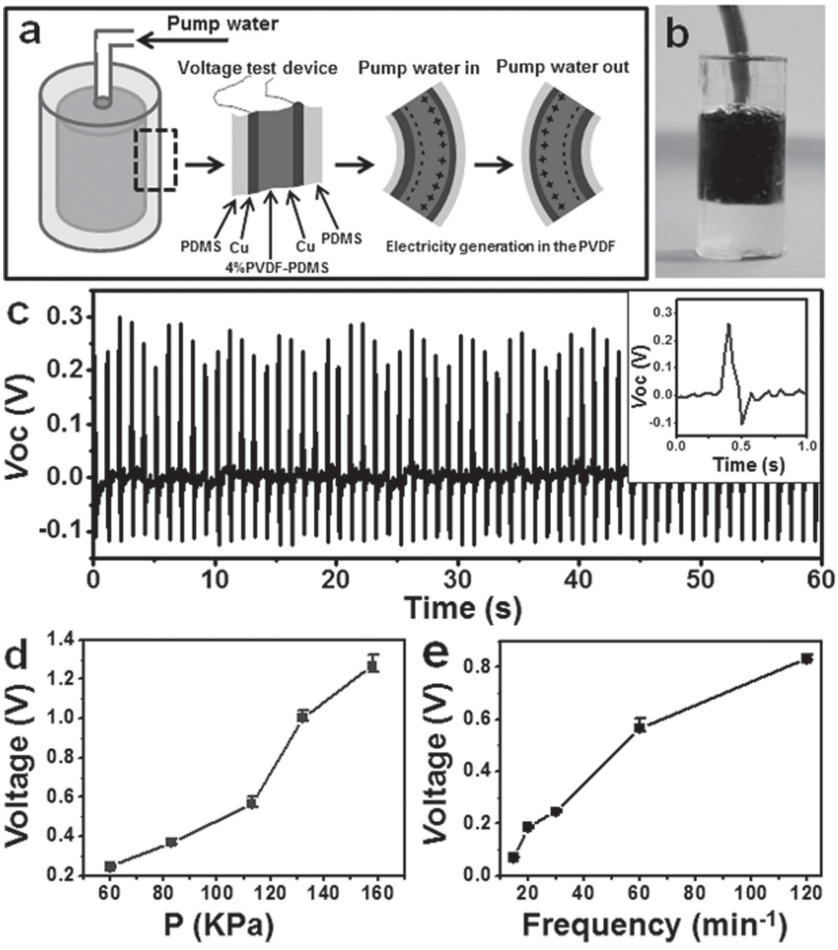

Figure 4. a) Schematic design of the artificial artery system with a PVDF-PDMS NG imbedded inside the wall to demonstrate the principle of harvesting energy from simulated blood pressure fluctuation. b) A digital photo of the artificial artery system filled with (blue) water simulating blood circulation. c) Piezoelectric voltage output profile when the liquid was pumped in and out from the artificial artery system. Inset is an enlarge profile of one single voltage peak showing good similarity to the real heart beating profile. d) Peak-to-peak V_{oc} obtained from the imbedded NG as a function of internal pressure difference. e) Peak-to-peak V_{oc} obtained from the imbedded NG as a function of pressure variation frequency.

4% PVDF. An output voltage of 2.87 V was recorded when the polymer NG slab was under an external force of 6 N. To further demonstrate the capability of harvesting mechanical energy from blood pressure fluctuation, an artificial artery system was fabricated with a PVDF-PDMS NG integrated inside. Under a simulated regular heart beating activity, an average ≈0.35 V peak-to-peak piezoelectric voltage output was achieved. The development of large-size porous piezoelectric PVDF with tunable mechanical property will show unprecedented application potential as an organ/muscle attachment or replacement for biomechanical energy harvesting, serving as a self-sufficient power source for implantable devices.

4. Experimental Section

Preparation of PVDF-PDMS Composite: PVDF was dissolved in DMSO at 70 °C under vigorous stirring to form a homogeneous solution. The amount of PVDF was weighted from 3% to 15% of the total mass. The solution was then stored at 12 °C for ≈2 h to form the gel. Porous PVDF was obtained by drying the gel at 18–25 °C, 0.8 Pa for 4–5 d, when the solid DMSO solvent was sublimated. The corresponding volume fraction of PVDF was ranged from 3% to 18%. The PDMS solution was prepared by mixing PDMS elastomer and crosslinker (Sylgard184, Dow Corning) with a 20:1 weight ratio. The porous PVDF network was immersed in the PDMS solution for 1 h. After degassing and thermal curing at 70 °C for 1 h, transparent flexible PVDF-PDMS composite was obtained. This method can be used to prepare the PVDF-PDMS composite film with a wide range of thickness from centimeters down to several micrometers.

NG and Artificial Artery System Fabrication: The PVDF-PDMS film NGs were fabricated with identical dimension (1 mm thickness, 0.2 cm^2 in area) with different PVDF volume fraction (3%–18%). Two pieces of copper foil with identical surface area were attached to the PVDF-PDMS slab as electrodes. The artificial artery system was fabricated using PDMS. PVDF composite NG was immersed in a tubular mold filled with PDMS solution. After degassing and thermal curing at 70 °C for 1 h, the artificial energy harvesting artery system was obtained. The system was filled with water and connected through a ¼ inch tube to a computer-controlled syringe pump to provide simulated blood pressure fluctuation.

Characterization: The morphology of PVDF was characterized by scanning electron microscope (LEO 1530). A nitrogen adsorption–desorption measurements (Quantachrome autosorb-1, quantachrome Instruments, FL, USA) was used to obtain the nitrogen physisorption isotherms at 77 K. Pore size distributions were obtained by applying density functional theory to the nitrogen adsorption isotherms. Transmittance measurements in the spectral range of 270–1000 nm were performed using a PE spectrum 18 spectrometer. FTIR was performed on the Bruker Tensor 27 spectrometer. Mechanical property of the PVDF-PDMS slabs was conducted on a Material Testing System (Model: QTest 5). To characterize the performance of NGs, the mechanical force was quantified by a Force Gauge HF-500N. To measure the piezoelectric output, the NG slab was placed on a flat hard surface with a mechanical force applied to the top surface at certain frequencies. The voltage outputs were recorded using an Agilent DSO1012A oscilloscope. The current outputs were measured using an Autolab PGSTAT302N station. The output voltage of the artificial artery system was measured by a Labview system controlled by the computer.

Supporting Information

Supporting Information is available from the Wiley Online Library or from the author.

Acknowledgements

Research reported in this publication was supported by the National Institute of Biomedical Imaging and Bioengineering of the National

Institutes of Health under Award No. R01EB021336. The content is solely the responsibility of the authors and does not necessarily represent the official views of the National Institutes of Health. Z.Z. thanks the support of Lin Guangzhao and Hu Guozan Graduate Education International Exchange Fund.

Received: May 26, 2016
Revised: June 23, 2016
Published online:

[1] X. D. Wang, *Nano Energy* **2012**, *1*, 13.
[2] X. Li, Z. H. Lin, G. Cheng, X. Wen, Y. Liu, S. Niu, Z. L. Wang, *ACS Nano* **2014**, *8*, 10674.
[3] S. H. Shin, Y. H. Kim, M. H. Lee, J. Y. Jung, J. H. Seol, J. Nah, *ACS Nano* **2014**, *8*, 10844.
[4] X. D. Wang, J. Song, J. Liu, Z. L. Wang, *Science* **2007**, *316*, 102.
[5] S. Lee, S. H. Bae, L. Lin, Y. Yang, C. Park, S. W. Kim, S. N. Cha, H. Kim, Y. J. Park, Z. L. Wang, *Adv. Funct. Mater.* **2013**, *23*, 2445.
[6] M. Yuan, L. Cheng, Q. Xu, W. Wu, S. Bai, L. Gu, Z. Wang, J. Lu, H. Li, Y. Qin, T. Jing, Z. L. Wang, *Adv. Mater.* **2014**, *26*, 7432.
[7] Y. F. Hu, Z. L. Wang, *Nano Energy* **2014**, *14*, 3.
[8] J. M. Donelan, Q. Li, V. Naing, J. A. Hoffer, D. J. Weber, A. D. Kuo, *Science* **2008**, *319*, 807.
[9] C. Dagdeviren, S. W. Hwang, Y. Su, S. Kim, H. Cheng, O. Gur, R. Haney, F. G. Omenetto, Y. Huang, J. A. Rogers, *Small* **2013**, *9*, 3398.
[10] L. Yin, X. Huang, H. Xu, Y. Zhang, J. Lam, J. Cheng, J. A. Rogers, *Adv. Mater.* **2014**, *26*, 3879.
[11] S. W. Hwang, C. H. Lee, H. Cheng, J. W. Jeong, S. K. Kang, J. H. Kim, J. Shin, J. Yang, Z. Liu, G. A. Ameer, Y. Huang, J. A. Rogers, *Nano Lett.* **2015**, *15*, 2801.
[12] K. I. Jang, H. U. Chung, S. Xu, C. H. Lee, H. Luan, J. Jeong, H. Cheng, G. T. Kim, S. Y. Han, J. W. Lee, J. Kim, M. Cho, F. Miao, Y. Yang, H. N. Jung, M. Flavin, H. Liu, G. W. Kong, K. J. Yu, S. I. Rhee, J. Chung, B. Kim, J. W. Kwak, M. H. Yun, J. Y. Kim, Y. M. Song, U. Paik, Y. Zhang, Y. Huang, J. A. Rogers, *Nat. Commun.* **2015**, *6*, 6566.
[13] C. Dagdeviren, Y. Shi, P. Joe, R. Ghaffari, G. Balooch, K. Usgaonkar, O. Gur, P. L. Tran, J. R. Crosby, M. Meyer, Y. Su, R. C. Webb, A. S. Tedesco, M. J. Slepian, Y. Huang, J. A. Rogers, *Nat. Mater.* **2015**, *14*, 728.
[14] M.-Y. Choi, D. Choi, M.-J. Jin, I. Kim, S.-H. Kim, J.-Y. Choi, S. Y. Lee, J. M. Kim, S. W. Kim, *Adv. Mater.* **2009**, *21*, 2185.
[15] D. Choi, M.-Y. Choi, W. M. Choi, H. J. Shin, H.-K. Park, J.-S. Seo, J. Park, S.-M. Yoon, S. J. Chae, Y. H. Lee, S.-W. Kim, J.-Y. Choi, S. Y. Lee, J. M. Kim, *Adv. Mater.* **2010**, *22*, 2187.
[16] D. Choi, M.-Y. Choi, H.-J. Shin, S.-M. Yoon, J.-S. Seo, J.-Y. Choi, S. Y. Lee, J. M. Kim, S.-W. Kim, *J. Phys. Chem. C* **2010**, *114*, 1379.
[17] H.-K. Park, K. Y. Lee, J.-S. Seo, J.-A. Jeong, H.-K. Kim, D. Choi, S.-W. Kim, *Adv. Funct. Mater.* **2011**, *21*, 1187.
[18] Z. H. Lin, Y. Yang, J. M. Wu, Y. Liu, F. Zhang, Z. L. Wang, *J. Phys. Chem. Lett.* **2012**, *3*, 3599.
[19] S.-H. Shin, Y.-H. Kim, M. H. Lee, J.-Y. Jung, J. Nah, *ACS Nano* **2014**, *8*, 2766.
[20] I. Babu, G. D. With, *Compos. Sci. Technol.* **2014**, *91*, 91.
[21] W. Wu, S. Bai, M. Yuan, Y. Qin, Z. L. Wang, T. Jing, *ACS Nano* **2012**, *6*, 6231.
[22] Y. J. Ko, D. Y. Kim, S. S. Won, C. W. Ahn, I. W. Kim, A. I. Kingon, S.-H. Kim, J.-H. Ko, J. H. Jung, *ACS Appl. Mater. Interfaces* **2016**, *8*, 6504.
[23] V. Bhavanasi, V. Kumar, K. Parida, J. Wang, P. S. Lee, *ACS Appl. Mater. Interfaces* **2016**, *8*, 521.
[24] C. Chang, V. H. Tran, J. Wang, Y.-K. Fuh, L. Lin, *Nano Lett.* **2010**, *10*, 726.
[25] C. Sun, J. Shi, D. J. Bayerl, X. D. Wang, *Energy Environ. Sci.* **2011**, *4*, 4508.
[26] S. Cha, S. M. Kim, H. Kim, J. Ku, J. I. Sohn, Y. J. Park, B. G. Song, M. Jung, E. K. Lee, B. Choi, J. J. Park, Z. L. Wang, J. M. Kim, K. Kim, *Nano Lett.* **2011**, *11*, 5142.
[27] Y. Mao, P. Zhao, G. McConohy, H. Yang, Y. Tong, X. D. Wang, *Adv. Energy Mater.* **2014**, *4*, 130624.
[28] P. Adhikary, S. Garain, D. Mandal, *Phys. Chem. Chem. Phys.* **2015**, *17*, 7275.
[29] D. Chen, J. X. J. Zhang, *Appl. Phys. Lett.* **2015**, *106*, 193901.
[30] A. Salimi, A. A. Yousefi, *Polym. Test.* **2003**, *22*, 699.
[31] J. F. Zheng, A. H. He, J. X. Li, C. C. Han, *Macromol. Rapid Commun.* **2007**, *28*, 2159.
[32] W. Joo, M. S. Park, J. K. Kim, *Langmuir* **2006**, *22*, 7960.
[33] J. Xie, J. Zhou, Y. C. Fung, *J. Biomech. Eng.* **1995**, *117*, 136.
[34] D. Y. Lee, H. Kim, H. M. Li, A. R. Jang, Y. D. Lim, S. N. Cha, Y. J. Park, D. J. Kang, W. J. Yoo, *Nanotechnology* **2013**, *24*, 175402.
[35] D. Dhakras, V. Borkar, S. Ogale, J. Jog, *Nanoscale* **2012**, *4*, 752.
[36] S. Cha, S. M. Kim, H. Kim, J. Ku, J. I. Sohn, Y. J. Park, B. G. Song, M. H. Jung, E. K. Lee, B. L. Choi, J. J. Park, Z. L. Wang, J. M. Kim, K. Kim, *Nano Lett.* **2011**, *11*, 5142.